Multifunctional Poly(Vinylidene Fluoride) and Styrene Butadiene Rubber Blend Magneto-responsive Nanocomposites Based on Hybrid Graphene Oxide and Fe_3O_4: Synthesis, Preparation and Characterization

Hamid Essabir (h.essabir@uiz.ac.ma)
National School of Applied Sciences of Agadir, Ibn Zohr University
Marya Raji
Institute of Nanomaterials and Nanotechnology (NANOTECH), Laboratory of Polymer Processing, Rabat
Denis Rodrigue
Université Laval, Quebec
Rachid Bouhfid
Institute of Nanomaterials and Nanotechnology (NANOTECH), Laboratory of Polymer Processing, Rabat
Abou el kacem Qaiss
Institute of Nanomaterials and Nanotechnology (NANOTECH), Laboratory of Polymer Processing, Rabat

Research Article

Keywords: Hybrid nanocomposite, Polymer blend, Graphene oxide, Magnetic nanoparticle, mechanical properties, electrical properties

Posted Date: March 24th, 2021

DOI: https://doi.org/10.21203/rs.3.rs-339953/v1

Abstract

Functional nanocomposites based on a blend of styrene butadiene rubber (SBR) and polyvinylidene difluoride (PVDF) as the matrix reinforced by a hybrid nanofiller system of graphene oxide nanosheets (GOn) and ferromagnetic nanoparticles (Fe_3O_4) at different weight ratios (3.75:1.25; 2.5:2.5 and 1.25:3.75) were successfully prepared and characterized to determine the effect of nanofillers hybridization in improving the structural,mechanical, dielectric/electrical, magnetic and thermal properties of a polymer blend (PVDF-SBR) for electromagnetic interference (EMI) shielding applications. Due to the synergy between both nanofillers, it was found that the Young's modulus of the nanocomposite containing 5 wt.% of the hybrid nanofiller was significantly improved (87%), while the strain at yield remained constant due to the low particle content and the rubbery effect of the SBR copolymer. In addition, the degradation temperature of the matrix was shifted from 464°C to 472 °C with the addition of 2.5:2.5 of GOn:Fe_3O_4. Finally, the hybrid reinforcement also had a positive effect on the electrical and magnetic properties of the nanocomposites with an improvement that exceeds 30%. By careful selection of synthetic techniques and understanding/exploiting the unique physics of the polymeric nanocomposites in such materials, novel functional polymer-inorganic nanocomposites can be designed and fabricated for new interesting in magneto applications such as superparamagnetism, electromagnetic wave absorption, and electromagnetic interference shielding.

Introduction

Recent research and development on functional materials revealed that the electromagnetic interference (EMI) shielding of materials has the potential to significantly improve specific applications such as lightning strike protection in airplanes, electronics field, sensors, as well as sensitive electronic devices, telecommunications, and radar systems. These systems generally emit electromagnetic waves generating some issues about the people's health and interference with the operation of near-by electronic devices. For these applications, conductive polymers are currently being investigated to protect sensitive equipment such as anti-electromagnetic interference coatings and appliances due to their lightweight with tunable conductive properties [1–3]. To this end, the development of nanocomposites based on a polymer matrix with nanofillers are expected to produce high mechanical properties as well as other important characteristics such as absorption/shielding, electrical conductivity and electric dipole, as well as magnetic dipoles. To further improve these properties, a hybrid particle system can be used to optimize several properties as the same time while improving other physical properties such as thermal stability [4, 5]. Furthermore, a polymer blend can be used as the matrix to combine several properties like strength, elasticity, etc. [6, 7]. The use of inorganic nanomaterials as fillers in a polymer matrix still show a growing interest due to their wide range of properties and potential industrial applications. Up to now, the majority of research focused on polymer nanocomposites reinforced with organized carbon materials such as carbon nanotubes (CNT), graphite and buckyballs [8–10]. These nanofillers have been promising materials because of their specific properties such as low density, small dimensions, high aspect ratio, as well as outstanding thermal and mechanical properties. Nevertheless, these developments generated new

challenges related to the nature and size of the reinforcements used such as the ones related to their dispersion/distribution, interfacial adhesion, availability, costs and stability, which are all critical factors to control the final properties and commercial success of a new nanocomposites [11–14].

Over the last years, two dimensional (2D) materials (graphene, phosphorene, silicene) became the subject of several scientific studies and their potential for the production of the next-generation of electronic and energy conversion devices. Since its discovery in 2004 by Geim and coworkers, graphene became an attractive material due to of its superior electrical, thermal, and mechanical properties [15, 16]. Graphene oxide nanosheets (GOn) can be obtained in large quantities from graphite using low-cost processes [17]. In the three-step graphene oxide synthesis, natural graphite is firstly oxidized into graphite oxide (GOn) using strong acids and oxidizing agents. Then, a simple sonication step in water or an organic solvent yields a stable GOn colloidal solution.

Magnetic stimulation has many advantages over other types of stimuli, especially in terms of penetration and invasiveness. Many materials (especially biological tissues) are much more transparent to magnetic fields than to electric fields, making it possible to remotely activate an event at a relevant distance from the magnet. To this aim, it is necessary to load the material of interest with structures able to produce a response to an external magnetic event Magnetic nanoparticles can be classified into five main types: ferromagnetic (iron, nickel, and cobalt), paramagnetic (gadolinium, magnesium, lithium, and tantalum), diamagnetic (copper, silver, gold), antiferromagnetic (MnO, CoO, NiO, and $CuCl_2$), and ferromagnetic (magnetite Fe_3O_4 and maghemite γ-Fe_2O_3) [4, 18, 19]. Recently, metallic iron oxide nanoparticles attracted a high interest due to their unique properties (magnetic, magneto-optical, magneto-resistive, thermal, electrical and mechanical properties) allowing them to be used in different applications including magnetic materials (circulators, oscillators and phase shifters for microwave regions), sensors, magneto-optical sensors, anodic materials for batteries, catalysts, sensors, phosphorescent laser sources, microwave and electrochemical devices, as well as black and brown pigments [20, 21]. The introduction of magnetic particles into a polymer offers a great potential for inspection since iron oxides have spontaneous magnetic induction. However, iron oxide nano-particles have a strong tendency to aggregate because of dipole-dipole interactions (so-called dipolar coupling) and free surface energy [20, 22]. Consequently, polymer blends are interesting to use for melt mixing as they can help to overcome this drawback due to selective localization of the nanoparticles at their interface of the matrix (if immiscible) which can be tuned according to the final application.

Nowadays, hybrid polymer nanocomposites are being used in an interesting range of applications. This class of materials offers several attractive characteristics such as ease of handling, high adaptability, as well as better thermal and mechanical properties combined with their low manufacturing costs. Furthermore, they are generally made from the hybridization of more than one type of reinforcements embedded in a polymer matrix to combine the advantages of all the components while compensating for the weakness of each one used individually [23, 24].

Several methods have been proposed to compound nanofillers in different polymer matrices. The main methods to get good dispersion/adhesion are: in situ polymerization, solution blending, and melt blending. One main disadvantage of in situ polymerization and solution blending is the use of organic solvent, which is usually very costly and not environmentally friendly. They are also limited in throughput (production rate) and involve extra steps (filtering, drying) and cost (solvent recovery). On the other hand, melt blending is considered more economical (continuous process) and flexible (process configuration and design), as well as being commonly used (industrial practice) [25, 26].

In our previous work, graphene oxide nanosheets as electrical conductive nanoparticles were incorporated into polyvinylidene fluoride (PVDF) using melt extrusion [13], as well as iron oxide (Fe_3O_4) nanoparticle as a magnetic filler into an acrylonitrile-butadiene-styrene/polyamide 6/styrene-butadiene rubber (ABS/PA6/SBR) blend [4]. The results showed that both nanoparticles were successfully dispersed into their respective polymer matrix, leading to improved thermal, mechanical and rheological properties at low nanoparticle content (3wt.%)[27]. In this work, the main objective is to develop a new multifunctional polymer nanocomposites for electromagnetic interference (EMI) shielding applications. The nanocomposite is based on a hybrid filler system of iron oxide (Fe_3O_4) as a magnetic filler and graphene oxide nanosheets (GOn) as an electrical conductive particle inside a polymer blend based on polyvinylidene fluoride/styrene-butadiene rubber (PVDF/SBR). Based on some preliminary work, the PVDF/SBR blend ratio was fixed at 65/35 wt.% leading to a good compromise between good flexibility and a low percolation thresholds from the formation of a conducting network throughout the polymer matrix. In particular, the effect of particle content on the tensile, hardness, thermal, rheological, electrical and magnetic properties of the nanocomposites are investigated.

1 Materials And Processing

1.1 Materials

The matrix was prepared by blending two polymers: polyvinylidene fluoride (PVDF) Kynar 1000HD purchased from Arkema (France) with a density of 1.77 g/cm^3 and a melting temperature of 177°C, with styrene-butadiene-rubber (SBR) supplied by Shell Chemical Company (Netherlands) with a density of 0.94 g/cm^3 and a melting temperature of 70°C. The PVDF/SBR ratio was fixed at 65/35 wt.%. All the other chemicals and solvents used were of analytical grade or of the highest purity available [28]. The natural graphite powder used to prepare the graphene oxide nanosheet was supplied by Sigma-Aldrich (France), as well as the concentrated sulfuric acid (H_2SO_4; 99%), hydrochloric acid (HCl; 5%), potassium permanganate (KMnO4; 99%), hydrogen peroxide (H_2O_2; 30%), and N,N-dimethylformamide (DMF, 99.8%). The iron oxide (Fe_3O_4) nanoparticles (NF) were obtained from Sigma-Aldrich (France) with a density of 5.1 g/cm^3 and a particle size under 50 nm [2].

1.2 Synthesis of graphene oxide nanosheets

Graphene oxide nanosheets (GOn) were obtained by the exfoliation of natural graphite, which ensures a large surface area and a high dispersion-distribution. The preparation steps are described as follows.

Graphene oxide (GO) was prepared according to the Hummers method. Graphite powder (2 g) was suspended firstly into cold (0°C, ice bath) concentrated sulfuric acid (50 mL) in a 250 mL round-bottom flask equipped with a magnetic stirrer bar. Then, 6 g of potassium permanganate (KMnO4) was slowly added with stirring and cooling to keep the temperature below 20°C. The mixing step was left for 2 h at 35°C, followed by the addition of distilled water (220 mL) and continuous stirring for an additional 15 min. Finally, the content of the flask was poured into distilled water (280 mL) with 15 mL of hydrogen peroxide (30%) to neutralize the permanganate excess (indicated by a color change of the solution from dark brown to yellow). The separation of graphite oxide from the liquid phase was done using distilled water and three times with a solution of HCl in water (1:10, vol/vol, dilution from commercial concentrated HCl (12.1 N) via a Thermo Scientific Sorvall WX Floor Ultra Centrifuges (10,000 rpm for 20 min) until the sulfates were no longer detected in the filtrate. The prepared graphite oxide was then exfoliated to obtain an aqueous colloidal suspension using sonication (Heated Ultrasonic bath Gun Cleaner, Germany) in 200 mL of N,N-dimethylformamide (DMF).

1.3 Processing

1.3.1 Matrix preparation

Firstly, the matrix (polymer blend) was prepared by mixing PVDF and SBR at a weight ratio of 65/35. The compounds were prepared on a Leistritz ZSE-18 (L/D = 40) twin-screw extruder operating at a screw speed of 125 rpm and a temperature profile of 220, 220, 230, 230, 220, 220, 220 and 220°C from the feed hopper to the circular die (3 mm). The extruded strands were then cooled in a water bath and pelletized (Thermo Fisher, UK).

1.3.2 Masterbatch preparation

Two masterbatch of PVDF/5 wt.% nanoparticles (GOn and Fe_3O_4) were prepared by solution-mixing in DMF using 22.5 g of PVDF dissolved in 250 mL of DMF inside a 1,000 mL round-bottom flask with stirring at 80°C in an oil bath. Stirring was performed until complete PVDF solubilization (about 60 min). A selected amount of GOn and Fe_3O_4 was mixed with 200 mL of DMF and treated with ultrasound for 45 min. Then, the PVDF solution was added to this suspension, and the mixture was stirred for 2 h at 80°C (oil bath). The suspension was poured into a large amount of distilled water, and a solid flocculent precipitated. The solid obtained after filtration was dried in a vacuum oven at 60°C for 8 h. The dried solid was finally crushed into a powder to obtain the masterbatch of PVDF/5 wt% (GOn at 5 wt.% and Fe_3O_4 at 5 wt.%). Figure 1 presents an overview of the complete processing steps for both nanoparticles.

1.3.3 Nano-composites preparation

The final hybrid nanocomposites were prepared by mixing the PVDF/GOn/Fe_3O_4 masterbatch with the matrix (PVDF/SBR blend) to get a final graphene oxide (GOn) and iron oxide (Fe_3O_4) concentration of 1.25, 2.5, 3.75 and 5 wt.% as summarized in Table 1. This was done on a Leistritz ZSE-18 (L/D = 40) twin-screw extruder operating at a screw speed of 125 rpm. The temperature profile was set at 220, 220, 230,

230, 220, 220, 220 and 220°C from the feed hopper to the circular die (3 mm). The material was finally pelletized (Thermo Fisher, UK) into pellets of 2–3 mm in length. Before molding, the pellets were oven-dried at 80°C for 24 h and finally processed via injection molding (Engel e-Victory). The injection temperature was fixed at 220°C with a mold temperature at 45°C.

Table 1
Formulation of hybrid nanocomposites produced.

Sample #	Ratio	PVDF/SBR (wt.%)	GOn (wt.%)	Fe_3O_4 (wt.%)
0	Neat matrix	65/35	0	0
1	5 :0	60/35	5	0
2	3.75 : 1.25	60/35	3.75	1.25
3	2.5 : 2.5	60/35	2.5	2.5
4	1.25 : 3.75	60/35	1.25	3.75
5	0 : 5	60/35	0	5

2 Characterization Techniques

The sample morphology and the level of nanofiller dispersion/distribution in the nano-composites were analyzed using a scanning electron microscope (SEM) (JEOL JSM 840A). To obtain clean and precise fractures, all the specimens were dipped in liquid nitrogen and cryogenically fractured before being coated by a thin conductive layer of Au/Pd. An ABB Bomem FTLA 2000 – 102 spectrometer (ATR: SPECAC GOLDEN GATE) was used to record the Fourier transform infrared spectra (FTIR) in the range of 400–4000 cm^{-1} with a resolution of 4 cm^{-1} and the accumulation of 16 scans. The thermal stability was evaluated by thermogravimetric analysis (TGA) via a Q500 instrument from TA Instruments (UK). Roughly 10 mg of each specimen was placed in a platinum pan and heated under air from room temperature to 800°C at a heating rate of 10°C/min. On the other hand, the mechanical (tensile) testing of five specimens for each nanocomposite with dimensions according to ISO 527-1:2012 [29], was performed using a universal testing machine Tinius Olsen (India) H10KT at a speed rate of 5 mm/min with a 5 kN load cell. For the dynamic rheological properties were obtained from a MCR 500 (Physica, Germany) rotational rheometer equipped with a CTD600 device (melt state). Small amplitude oscillatory shear (SAOS) tests were carried out at 180°C using a 25 mm parallel plate geometry with 2 mm thick samples. Frequency sweeps from 500 Hz to 0.05 Hz were performed with a strain amplitude of 5%, for which the materials exhibit a linear viscoelastic behavior as verified by previous strain sweeps at 1 Hz. For the electrical resistivity measurement, an electrometer/high resistance meter (Keithley instruments, 6517B) coupled to a Keithley 8009 resistivity test fixture for short electrification time was used. This system is a guarded test fixture to determine the volume and surface resistivity, generally able to supply high electrostatic shielding and high insulation resistance up to 1100 V. The samples had an average diameter of 9 cm and 1 mm thick. The magnetic properties were determined by the force necessary to remove the

nanocomposite samples from a magnet [27]. This test setup was developed in our lab and the characterization was made using the same tensile machine as for the tensile properties, by changing the fixture by a homemade system as shown in Fig. 2. The assembly contains two supports where a magnet is fixed on the bottom plate and the sample is fixed (glued to the support by double-sided tape) on the top plate. The complete set-up is then mounted on the universal testing machine grip (Fig. 2). Both the sample and the magnet have dimensions of (36 × 16 × 1) mm^3. The magnetic strength (σ) was determined as:

$$\sigma = F / S \quad (1)$$

where F is the necessary force to detach the samples from the magnet, and S is the sample surface (cross-section).

3 Results And Discussion

3.1. Scanning electron microscope (SEM)

Figure 3 shows the SEM morphology of the cryo-fractured PVDF-SBR blend matrix and its nanocomposites for GOn/Fe_3O_4 at (2.5/2.5). The neat PVDF-SBR (65/35) blend shows a plain type morphology (absence of nanofillers).

It can be easily seen that the morphology of neat PVDF-SBR blend polymer is a sea-island morphology with a large amount of droplet phenomenon and droplet size close to 40 μm which confirms that both polymers are immiscible due to the rough appearance of the rubber component of the SBR [2, 16]. On the other hand, Fig. 3b, shows that the addition of nanofillers (GOn-Fe_3O_4) at 2.5 wt.% may decrease the size of droplets to the average diameter of 18μm leading to a formation of finer morphology with the presence of lower amount of pullout phenomenon as compared of neat PVDF-SBR material that may be ascribed to compatibilizing effect of nanofillers via the physical interaction. The morphology of hybrid nanocomposites starts to transform in a co-continuous structure with the presence of highly dispersed a small droplet with a size of 18 μm and the appearance of some dispersed nanosheet (GnO) and nanoparticles (Fe3O4) of PVDF-SBR with a size around of 7 − 6 μm. This structure is due to the coalescence suppression of phase-separated domains trough the formation of physical interaction between the polymer components via nanofillers [30]. For the Fig. 3 (b'), the morphology of the hybrid nanocomposite PVDF-SBR/GOn-Fe_3O_4 at (2.5/2.5) sample shows that good dispersion/distribution of the nanofillers was obtained as no traces of agglomeration can be seen. The presence of agglomeration would indicate poor affinity and lower distribution homogeneity [31, 32]. In our case, the GOn and Fe_3O_4 nanoparticles are homogeneously distributed due to the functional group interaction between both nanofillers. The oxygen content in the functional groups on the GOn surface can interact with the Fe_3O_4 nanoparticles via hydrogen bonding as well as van der Waals interactions, resulting in good dispersion of the nano-fillers inside the PVDF. Moreover, it is clearly shown on Fig. 3(a',b') that good interfacial adhesion was produced after the nanofillers incorporation since no deboning can be seen. Finally, the nanofillers

are well dispersed inside the matrix and it can be concluded that the masterbatch approach and the processing conditions used were optimum leading to good dispersion/distribution and uniform nanocomposite properties[33].

3.2. Fourier transform infrared spectroscopy (FTIR)

Fourier transform infrared (FTIR) spectroscopy is an effective method to study possible crystalline phase transformation in PVDF. Figure 4 shows the FTIR spectra of the neat PVDF-SBR blend and the PVDF-SBR nanocomposites at different GOn and Fe_3O_4 content. The FTIR spectra of the neat matrix is composed of the two main characteristic bands of both PVDF and SBR. The characteristic bands of SBR are located at 3040 – 3020 cm^{-1} corresponding to C–H stretching, the band at 1479 cm^{-1} corresponds to CH_2 in-plane deformation, and 1376 cm^{-1} band is characteristic of $–CH_2$ wagging motion; while the PVDF has its main characteristic bands at 975, 720, 672, 659 and 469 cm^{-1} which are specific to the presence of the pure α-phase. The bands at 975 cm^{-1} corresponds to CH_2 rocking, the band at 720 cm^{-1} is characteristic of bending and skeletal bending, the bands at 672 – 659 correspond to CF_2 groups and rocking vibration, and the band at 469 cm^{-1} is associated to CF_2 bending. From this analysis, it is clear that the PVDF blended with the SBR is only only showing the α-phase, similar to the pure PVDF.

It is clear from the FTIR spectra of the nanocomposites that new bands are presents compared to those of the PVDF α-phase, depending on the GOn, Fe_3O_4 or GOn-Fe_3O_4 content (wt.%). They are localized at 1218 – 1178, 966, 907, 869, 600, 568, and 437 cm^{-1} which are assigned to the β-polymorph structure of PVDF. This confirms that nanoparticles addition led to some PVDF crystal transformation from the α-phase to the β-phase as reported in the literature [27]. The increase of the β-phase content in the nanocomposite can be related to the presence of GOn and Fe_3O_4 nanoparticles providing additional nucleation sites (heterogeneous nucleation) for the crystallization of the β-phase. The formation of the β-polymorph in the PVDF-SBR nanocomposites is also attributed to the strong and specific interaction between the carbonyl groups in graphene oxide and the fluoride groups in PVDF (-C-O) found in graphene oxide and the CF_2 segments of PVDF leading to a transformation from the α-phase's trans-gauche-trans-gauche conformation into the trans-trans conformation characteristic of the β-phase. These results confirm the presence of a mixture of α- and β-polymorph in the PVDF-SBR nanocomposites studied. Among the observed polymorphs, the polar β phase of PVDF is the most desirable form because of its high permittivity making it a good candidate for piezoelectric material based on polymer matrices[27, 34].

3.3. Thermal properties:

The thermal resistance of the PVDF-SBR blend and its nanocomposites was evaluated using TGA. Figure 5 presents the weight curves a function of temperature at a heating rate of 10°C/min in air. It can be seen that all the curves have a similar shape, but the thermal stability increases with the presence of the nanoparticles. This is especially the case when compared with the neat PVDF matrix in the temperature range of 300–800°C. The nanocomposites filled with Fe_3O_4 alone (5 wt.%) show the highest

thermal stability compared to the nanocomposites filled with GOn alone at the same content. This can be related to the higher intrinsic thermal stability of iron oxide compared to the graphene oxide nanoplatelets [35].

The temperature associated to the maximum degradation rate (Tmax) was obtained by the position of peak in the derivative thermogravimetric curve (DTG). Based on the DTG curve of the neat matrix (PVDF-SBR), it is clear that two maxima are present, which are associated to both polymers; the first one corresponds to SBR (437°C) and the second one is PVFD (464°C). It is clear in Fig. 5 that the Tmax of the nanocomposites is higher than that of the neat PVDF-SBR matrix. The Tmax of PVDF-SBR matrix is 464°C and increases to 470 ^{o}C and 477°C for the 5 wt % GOn and Fe_3O_4 nanocomposites, respectively. On the other hand, Tmax of the hybrid system (GOn:Fe_3O_4 at 2.5:2.5) shows an intermediate value (472°C). From these results, it clear that the incorporation of GOn and Fe_3O_4 nanoparticles in the PVDF-SBR blend matrix induced better thermal stability and thus the starting decomposition temperature is shifted to higher temperatures. During thermal degradation, GOn and Fe_3O_4 nanofillers, due to their inorganic nature, with the homogeneous distribution and distribution of nanofillers prevent the evolution of volatile decomposition products acting as a barrier inhibiting the propagation of heat from the environment in the polymer matrix [36, 37]. On the other hand, there is a close relationship between the crystallin phase of PVDF and the obtained results regarding the increased thermal stability. The addition of GOn or Fe_3O_4 (alone or together) leads to additional nucleation sites for the crystallization of the β-phase of PVDF leading to PVDF crystal transformation from the α-phase to the β-phase. In general, the crystaline phase has a higher thermal stability compared to the amorphous phase due to the ordered structure leading to a highest energy dissipation [27]. Finally, GOn and Fe_3O_4 can act as nucleating agent, as well as thermal stabilizers.

3.4. Tensile testing

The large aspect ratio of the GOn and Fe_3O_4 nanoparticles and their respectively high Young's modulus should have a significant reinforcement effect on the mechanical properties of the PVDF-SBR blend [3, 22, 23]. The homogenous dispersion/distribution of the nanofillers into the matrix, along with favorable interfacial interactions between the nanofillers and the polymer blend, as well as the high level of exfoliation of GOn are the key points to achieve polymer nanocomposites with highly enhanced final properties[40, 41].

The tensile properties of neat PVDF-SBR blend and its nanocomposite were investigated by uniaxial tensile testing. Figures (6) presents the Young's modulus, tensile strength, and strain at yield as a function of GOn and Fe_3O_4 content. Firstly, the neat PVDF, neat SBR and PVDF-SBR blend tensile properties are reported in Table 2. From these results, it is clear that SBR has better elasticity (higher strain at yield) compared to PVDF which is more rigid (higher modulus and strength). So the properties of the blend are in between. In our case, one of the main goal is to produce rigid nanocomposites while maintaining some ductility. So Fig. 6a shows that the addition of GOn and Fe_3O_4 nanoparticles gradually changes the tensile properties of the PVDF-SBR blend for the range of Fe_3O_4 loading (1.25-5 wt.%) investigated. But

the nanocomposite containing only 5 wt.% Fe_3O_4 showed better mechanical properties with respect to the nanocomposite containing 5 wt.% GOn and the neat matrix. The Young's modulus of these nanocomposites (1.25, 2.5 and 5 wt.% Fe_3O_4) was increased by around 85% compared to the neat PVDF-SBR matrix and the nanocomposite with 5 wt.% GOn. Higher Young's modulus with Fe_3O_4 is due to the intrinsic properties of this nanoparticles compared to the nanosheet in terms particle shape. The sheet shape of GOn prevents their dispersion and distribution into the polymeric matrix at higher loading. So the GOn start to aggregate for content above 2.5 wt.%, while for Fe_3O_4 with their particulate shape (more spherical), there is a good dispersion and distribution into the matrix even up to 5 wt.% [42, 43].

When particle hybridization was performed by combining Fe_3O_4 and GOn, it can be seen that all the nanocomposites exhibit superior Young's modulus than for the nanocomposites based on GOn or Fe_3O_4 alone. This confirm that a synergistic effect occurs between both particles leading to better reinforcement of the PVDF-SBR matrix. The results also show that by decreasing the GOn content and increasing the Fe_3O_4 nanoparticles (fixed total content), the Young's modulus gradually increase to reach a maximum value (2052 MPa) at a GOn:Fe_3O_4 of 2.5:2.5 wt.% before decreasing. So this hybrid nanocomposites presents the optimum results due to the synergetic effect induced by the combination of GOn and Fe_3O_4 [23],[44]. Such synergistic interactions result in the formation of an homogeneous interconnected network structure, which explains the large increase in the matrix Young's modulus. On the other hand, the phenomenon of nanosheets restacking at GOn:Fe_3O_4 of 2.5:2.5 wt.% does not occur and the nanosheets are still well dispersed and distributed within the matrix. Actually, the GOn surface becomes decorated with Fe_3O_4, which inhibited the sheet-to-sheet aggregations of GOn as evidenced by SEM observations in Fig. 3; i.e. no aggregation of sheets or nanoparticles was observed, ascribed to the good processing conditions used leading to high distribution and dispersion level of GOn and Fe_3O_4 combined with the strong hydrogen bonding between the matrix and the surface of GOn and Fe_3O_4 [44]. For the nanocomposites containing only one type of particle (GOn or Fe_3O_4) at 5wt.%, the relatively lower Young's modulus can be associated to the possible agglomeration of some nanosheets. These agglomerates may prevent an efficient interfacial load transfer and changes in the fillers aspect ratio [23, 45].

Figure 6a also shows the tensile strength of the nanocomposites as a function of nanoparticles content. It is clear from Fig. 6a that a slight tensile strength decrease (5%) is observed for all the nanocomposites compared to the neat matrix. Generally in nanocomposites, an increase of the nanofillers content combined with a weak interfacial adhesion between the nanofillers and the matrix leads to poor interfacial quality and more decohesion zone are created in the nanocomposites under stress. This decohesion acts as stress concentration points accelerating sample failure [46]. On the other hand, it is observed that the tensile strength of all the nanocomposites are similar close to 44.7 MPa (± 0.2 MPa). This result may confirm the good interfacial adhesion generating better stress transfer under tensile load; i.e. better compatibility and affinity between GOn and Fe_3O_4 with the matrix. This is especially the case for the hybrid nanocomposites as the tensile strength is almost constant independent of the GOn:Fe_3O_4 ratio. The interfacial adhesion between the GOn:Fe_3O_4 hybrid system and the polymer matrix was very

good as confirmed by SEM images (Fig. 3). As a results, the GOn:Fe_3O_4 hybrid nanofiller network acts as an efficient reinforcement in the parent system, providing superior tensile properties to the nanocomposites. In this case, effective stress transfer occurred from the polymer chains to the dispersed hybrid nanofiller, providing additional strength to the nanocomposites attributed to the synergistic effect generated from the combination of GOn and Fe_3O_4. Therefore, the successful addition of a relatively high nanofiller content into the polymer matrix strongly depends on the good compatibility and the strong interfacial interaction between all phases present.

Change in the ductile behavior of the nanocomposites related to GOn and $F_{e3}O_4$ content and their hybridization was also investigated according to the strain at yield results. Figure 6b shows that the strain at yield of the nanocomposites gradually decreased with nanofillers loading. The strain at yield decreased to 20% for all the nanocomposites compared to the blend matrix. However, an almost contant value of the strain at yield values around 0.41 mm/mm (± 0.01 MPa) is observed for all the hybrid nanocomposites. Lower strain at yield for the nanocomposites was expected because of the intrinsic rigid character of both nanoparticles which have low deformation and act as stress concentrators accelerating crack initiation. The nanofillers used, even at lower content, also acted as nucleating agents reducing the amount of plastic energy (elasticity) absorbed by the nanocomposites under stress leading to lower ductility [47]. Another reason for the low ductility of the nanocomposites is due to the large aspect ratio and the strong interactions between the GOn and Fe_3O_4 with the matrix, which increased the crystallinity, both imposing restriction on the polymer chains mobility [48]. However, the almost constant strain at yield of all the nanocomposites, even with the increased of rigidity, is mainly due to the effect of the elastomeric nature of the SBR which confers the ductile behavior of the nanocomposites by preventing crack propagation along the interfacial area and facilitates mechanical energy dissipation. Furthermore, SBR addition led to maintain the strain at yield as it increases the interfacial adhesion improving the stress transfer to the nanofillers and promoting an efficient distribution of the applied stresses.

Such improvement in mechanical properties for the hybrid nanocomposites at a GOn:Fe_3O_4 ratio of 2.5:2.5 wt.% can be related to the good dispersion of GOn and Fe_3O_4, which is related to the high compatibility between all the phases, as well as the presence of strong hydrogen-bonding interactions between the polymer matrix chains and the nanofillers generating a strong synergy between GOn, Fe_3O_4, and PVDF-SBR. All these effects are required to improve the interfacial stress transfer from the polymer matrix to the individual nanofillers, thus increasing the nanocomposite mechanical properties.

Table 2
Tensile properties of the used polymers.

Polymer	Young's modulus (MPa)	Tensile strength (MPa)	Strain at yield (mm/mm)
PVDF	1500	50	0.15
SBR	40	25	2.5
PVDF/SBR (65/35)	1098	46.9	0.5

3.5. Rheological properties:

The dynamic rheological properties of the nanocomposites were measured to provide further information on the internal structure and processability of these materials. Moreover, the information on the nanofillers dispersion state (percolated network structure), the effect of rigid particle addition on the motion of polymer chains, and interaction between the components can also be extracted.

Figure 7 compares the rheological properties of the nanocomposites in the melt state. It can be seen that the nanofiller content and frequency play an important role in the materials response to dynamic stress. Firstly, the addition of GOn or Fe_3O_4 into the polymer matrix disturbs the mobility of the polymer chains in the melt, thus increasing the storage modulus and loss modulus of the nanocomposites compared to the neat matrix. This also confirms the reinforcement effect of the nanofillers. The presence of rigid nanoparticles limits the polymer chain mobility and changes their molecular dynamics [49, 50]. Thus, large-scale polymer chain relaxation in the nanocomposites was effectively restrained by the presence of rigid inclusions. On the other hand, it is clear that the nanocomposites containing Fe_3O_4 alone (5 wt.%) produced significantly higher storage modulus than their GOn counterparts (5 wt.%). This behavior indicates that the nanofiller type has a direct effect of this property, as for the tensile properties (Fig. 5). This can again be related to the particle shape and their interactions with the matrix.

Figure 7 also shows that all the hybrid nanocomposites have intermediate values of storage modulus and loss modulus, between that of GOn and Fe_3O_4 nanocomposites. The synergetic effect induced by the combination of both particles is more effective in restraining the polymer relaxation than using GOn or Fe_3O_4 alone. This is due to the higher surface area and higher aspect ratio when two nanofillers are combined (better organization). Together with the high surface area of Fe_3O_4 and the nanoscale flat surface of GOn, the hybrid system led to stronger interfacial interactions with the matrix, good distribution/dispersion, and substantially higher effect on the polymer chain motion.

Figure 7 clearly show that the rheological properties of the nanocomposites have a predominantly elastic behavior at high frequencies (G' > G"), while a more viscous behavior is observed at low frequencies (G' < G"). This transition is associated to the polymer chains relaxation time [51]. The frequency also plays an important role on the nanocomposites' rheological response which is related to the viscoelastic behavior of these materials; i.e. a more solid-like behavior at higher frequencies as there is not enough time for the

chain entanglements to occur and follow the deformation imposed, so a small amount of relaxation results in a higher value of the storage modulus (G'). On the other hand, the low-frequency region is related to reptation relaxation which is the motion of the whole chain [52].

One of the most important properties of thermoplastics materials is their viscosity which is a key property for successful manufacturing. The viscosity allows to predict flow of material inside processing equipment like extrusion and injection machines. It also allows to optimize the processing parameters (temperature, flow rate, screw speed, etc.) to produce homogeneous and stable parts [53]. Generally, viscosity is a function of the number of effective chains participating in the formation of a network structure. Figure 7c shows the complex viscosity as a function Gon and Fe_3O_4 content, and frequency. The results show an increase in complex viscosity with the addition of GOn at 5 wt.% to reach a maximum for the nanocomposites containing Fe_3O_4 nanofillers (5 wt.%). However, all the hybrid nanocomposites show intermediate values. The increased complex viscosity at low frequency of all the nanocomposites compared to the neat matrix can be attributed to the nanoscale dispersion/distribution of the nanofillers and to the presence of a higher number of interacting chains resulting from strong interfacial adhesion [54].

It can also be seen in Fig. 7c that the complex viscosity decreases with increasing frequency due to the strong shear-thinning behavior of polymers in the a melt state [55, 56]. A significant increase in the complex viscosity (η*) of the nanocomposites with increasing GOn and/or Fe_3O_4 content can be seen. The effect of the nanofillers content is mostly seen at low frequency, and the relative effect decreases with increasing frequency because of shear thinning behavior. The entanglement of polymer chains hinders the shear flow at a lower frequency, therefore higher viscosity is observed. But lower viscosity makes easier the processing and blending of nanocomposites at higher nanofiller content.

3.6. Electrical properties:

One of the key challenges to fabricate thermoplastic nanocomposites with high electrical and mechanical properties is related to the good processing conditions leading to the production of an interconnected network of nanofillers. Electrical percolation in conducting polymer nanocomposites containing nanofillers is strongly dependent on the properties of the nanofiller, namely their aspect ratio (L/D), electrical properties, and dispersion, as well as the nanocomposite microstructure associated to the dispersion and orientation of the nanofiller within the polymer matrix [57]. The addition of GOn and/or Fe_3O_4 has an effect on the electrical conductivity of the polymer matrix because of the intrinsic electrical properties of graphene and iron oxide which can provide percolated pathways for electron transfer making the nanocomposites electrically conductive even at low content [58, 59].

The effect of nanofillers on the electrical conductivity of the PVDF-SBR matrix is shown in Fig. 8. From the results obtained, it is clear that the electrical conductivity was influenced by the addition of 5 wt.% GOn, 5 wt.% Fe_3O_4 and 5 wt.% GOn:Fe_3O_4 hybrid nanofillers at various ratios. The electrical conductivity in Fig. 8 show an increases from $4.37x10^{-13}$ S/m for the neat PVDF-SBR matrix to $1.71x10^{-11}$ and 7

$x10^{-12}$ S/m for 5 wt.% GOn and 5 wt.% Fe_3O_4 nanocomposite, respectively. The nanocomposites with GOn alone had higher electrical conductivity than nanocomposites with Fe_3O_4 alone because of the higher aspect ratio of GOn. The percolation theory describes the connectivity of objects within a network structure and the effects of this connectivity on the macroscale properties of the system [60]. The nanofillers with nanoscopic dimensions and thereby large surface area to volume ratios tend toward agglomeration due to the strong interparticle attractive forces. This is particularly true for GOn that experience high van der Waals interlayers interactions. This intrinsic attraction, coupled with their high aspect ratios, can lead to substantial GOn aggregation. In addition to the nanoscale bundling or clustering of the nanofillers, the micro- and macro-scale dispersion/distribution is affected by both the internal inter-nanofillers and nanofillers interactions and by the external forces applied during the nanocomposite fabrication. The details of the nanofillers microstructure significantly affect the electrical properties of the final nanocomposite and give more advantage to the nanocomposites based on GOn.

The electrical conductivity of the nanocomposites containing hybrid nanofillers is higher than Fe_3O_4 nanocomposites at the same nanofiller content. However, the results show that the hybrid nanocomposites GOn:Fe_3O_4 -2.5:2.5 has an intermediate value ($1.10x10^{-11}$ S/m). As a result, the synergistic effect between GOn and Fe_3O_4 makes it possible for the partial replacement of the high aspect ratio and high-cost nanofillers (GOn) with low aspect ratio and lower cost Fe_3O_4.

3.7. Magnetic properties

Figure 9 presents the magnetic properties of the nanocomposites as measured by the system described in Fig. 2. The set-up determines the force (stress) necessary to detach the nanocomposites from a magnet. The measured magnetic stress presented in Fig. 9 shows that all the nanocomposites containing Fe_3O_4 alone at 5wt.% and GOn:Fe_3O_4 hybrid nanofillers exhibit superior magnetic properties than those observed for the nanocomposite containing GOn at 5wt.% alone. The magnetic stress increases linearly from 0 Pa for the GOn nanocomposites to reach a maximum of 870 Pa for the Fe_3O_4 nanocomposites at 5 wt.%. This increase with Fe_3O_4 content confirms the ferromagnetic behavior of the nanocomposites, which is attributed to the magnetic properties of the Fe_3O_4 nanoparticles and to the good dispersion/distribution of the magnetic nanofillers inside the polymer matrix confirmed by SEM (Fig. 3) and mechanical (Fig. 6) results [4, 61].

For the hybrid nanocomposites, the magnetic stress increased with increasing Fe_3O_4 ratio. At low nanofillers content, the nanocomposites are superparamagnetic due to the directions of weak magnetization axes which are randomly distributed [62, 63]. However, at high concentration, a interaction between the nanofillers occurs to form an infinite conductive network leading to ferromagnetic properties. The advantage of introducing magnetic nanoparticles in a material is twofold, as magnetic field gradients can be used to move the material, while alternating magnetic fields can be used to locally heat up the regions in the proximity of Fe_3O_4 .As the size of magnetic particles is reduced below a critical

diameter (typically in the order of tens of nm), particles behave as superparamagnets[64] i.e., the atomic moments of the nanoparticle are aligned into a giant magnetic moment.

Once again for the magnetic properties, the hybrid system is an excellent way to produce nanocomposites with good magnetic properties, but good distribution/dispersion of the nanofillers in the matrix is required, which also leads to higher mechanical properties.

4 Conclusion

In this work, the combination of graphene nanosheets (GOn) and ferromagnetic iron oxide nanoparticles (Fe_3O_4) was used to produce a novel hybrid nanofiller system which was highly effective to overcome the agglomeration phenomenon. In particular, a PVDF/SBR blend was used as the matrix to get a balance between rigidity and ductility. Three GOn:Fe_3O_4 ratio were used to compared with the properties of each nanoparticle used alone.

The results showed a significant improvement in structural, thermal, mechanical, rheological, electrical and magnetic properties of the hybrid nanocomposites due to strong interfacial interaction and a synergistic effect from the combination of both kinds of nanofiller (GOn and Fe_3O_4). The synergistic effect of 2D exfoliated GOn with 1D Fe_3O_4 nanoparticles improved the dispersion/distribution homogeneity by avoiding agglomeration phenomenon within the polymer, resulting in nanocomposites with enhanced properties. Based on the results obtained, it is now possible to develop novel multifunctional nanocomposites based on the combination of existing nanomaterials. The possibilities are enormous, especially for conductive applications like electronics, sensors, energy harvesting and storage, as well as other more general properties like electromagnetic interference (EMI) shielding and radar/infrared blocking.

Declarations

Acknowledgments

This work was supported by MAScIR; Moroccan Foundation for Advanced Science, Innovation and Research, MESRSFC and CNRST, Morocco grant no. 1970/15. Authors would like to thank Mr. Mehdi Ait Dahi for his fruitful technical support and assistance.

Ethical Approval

This research does not deal with human subjects, so we do not need an Ethical Approval.

Consent to Participate

This research does not deal with human subjects, so we do not need informed consent to Participate.

Consent to publish

This statement is to certify that all authors have seen and approved the manuscript being submitted. We warrant that the article is the authors' original work. We warrant that the article has not received prior publication and is not under consideration for publication elsewhere. On behalf of all co-authors, the corresponding author shall bear full responsibility for the submission.

The authors declare that there is no conflict of interest.

Funding

The author(s) received no financial support for this research.

Competing Interests Statement

Article/Work Title: Multifunctional poly(vinylidene fluoride) and styrene butadiene rubber blend Magneto-responsive nanocomposites based on hybrid graphene oxide and Fe3O4: Synthesis, preparation and characterization

Author contribution statements

Hamid Essabir wrote the manuscript, fabricated the sample, conceived and planned the experiments, verified and discussed the results, with support from Marya Raji.

Marya Raji Discussed the results and contributed to the final manuscript .

Denis Rodrigue helped supervise the project and the discussed results and contributed to the final manuscript.

Rachid Bouhfid and Abou el kacem Qaiss conceived and planned the experiments, conceived the original idea, helped supervise the project and contributed to the final manuscript.

Availability of data and materials

Data not available due to ethical restrictions

References

1. Zhang H, Verberne P, Meguid SA, et al (2020) Autonomous high resolution inspection of kiss-bonds skins of carbon nanotube reinforced nanocomposites using novel dynamic line-scan thermography approach. Compos Sci Technol 192:108111. https://doi.org/10.1016/j.compscitech.2020.108111
2. Agrawal PR, Kumar R, Teotia S, et al (2019) Lightweight, high electrical and thermal conducting carbon-rGO composites foam for superior electromagnetic interference shielding. Compos Part B Eng 160:131–139. https://doi.org/10.1016/j.compositesb.2018.10.033
3. Bai H, Ge G, He X, et al (2020) Ultrahigh breakdown strength and energy density of polymer nanocomposite containing surface insulated BCZT@BN nanofibers. Compos Sci Technol

195:108209. https://doi.org/10.1016/j.compscitech.2020.108209

4. Essabir H, Raji M, Essassi EM, et al (2017) Morphological, thermal, mechanical, electrical and magnetic properties of ABS/PA6/SBR blends with Fe3O4 nano-particles. J Mater Sci Mater Electron 28:17120–17130. https://doi.org/10.1007/s10854-017-7639-2
5. Pourjavadi A, Rahemipoor S, Kohestanian M (2020) Synthesis and characterization of multi stimuli-responsive block copolymer-silica hybrid nanocomposite with core-shell structure via RAFT polymerization. Compos Sci Technol 188:107951. https://doi.org/10.1016/j.compscitech.2019.107951
6. Chizari K, Arjmand M, Liu Z, et al (2017) Three-dimensional printing of highly conductive polymer nanocomposites for EMI shielding applications. Mater Today Commun 11:112–118. https://doi.org/10.1016/j.mtcomm.2017.02.006
7. Polfus JM, Jayasayee K (2019) Robust nanocomposites of α-Fe2O3 and N-doped graphene oxide: Interfacial bonding and chemisorption of H2O. Carbon N Y 152:497–502. https://doi.org/10.1016/j.carbon.2019.05.033
8. Nouri N, Rezaei M, Mayan Sofla RL, Babaie A (2020) Synthesis of reduced octadecyl isocyanate-functionalized graphene oxide nanosheets and investigation of their effect on physical, mechanical, and shape memory properties of polyurethane nanocomposites. Compos Sci Technol 194:108170. https://doi.org/10.1016/j.compscitech.2020.108170
9. Naeem M, Kuan H-C, Michelmore A, et al (2020) A new method for preparation of functionalized graphene and its epoxy nanocomposites. Compos Part B Eng 108096. https://doi.org/10.1016/J.COMPOSITESB.2020.108096
10. Guillet JF, Valdez-Nava Z, Golzio M, Flahaut E (2019) Electrical properties of double-wall carbon nanotubes nanocomposite hydrogels. Carbon N Y 146:542–548. https://doi.org/10.1016/j.carbon.2019.01.090
11. Essabir H, Raji M, Laaziz SA, et al (2018) Thermo-mechanical performances of polypropylene biocomposites based on untreated, treated and compatibilized spent coffee grounds. Compos Part B Eng 149:. https://doi.org/10.1016/j.compositesb.2018.05.020
12. Kakou CA, Essabir H, Bensalah M-O, et al (2015) Hybrid composites based on polyethylene and coir/oil palm fibers. J Reinf Plast Compos 34:1684–1697. https://doi.org/10.1177/0731684415596235
13. Raji M, Essabir H, Rodrigue D, et al (2017) Influence of Graphene Oxide and Graphene Nanosheet on the Properties of Polyvinylidene Fluoride Nanocomposites. Polym Polym Compos. https://doi.org/10.1002/pc
14. Malha M, Nekhlaoui S, Essabir H, et al (2013) Mechanical and thermal properties of compatibilized polypropylene reinforced by woven doum. J Appl Polym Sci 130:4347–4356. https://doi.org/10.1002/app.39619
15. Minář J, Brožek J, Michalcová A, et al (2019) Functionalization of graphene oxide with poly(ε-caprolactone) for enhanced interfacial adhesion in polyamide 6 nanocomposites. Compos Part B

Eng 174:107019. https://doi.org/10.1016/j.compositesb.2019.107019

16. Peretz Damari S, Cullari L, Nadiv R, et al (2018) Graphene-induced enhancement of water vapor barrier in polymer nanocomposites. Compos Part B Eng 134:218–224. https://doi.org/10.1016/j.compositesb.2017.09.056
17. Najafi F, Wang G, Mukherjee S, et al (2020) Toughening of graphene-based polymer nanocomposites via tuning chemical functionalization. Compos Sci Technol 194:108140. https://doi.org/10.1016/j.compscitech.2020.108140
18. Sang G, Dong J, He X, et al (2019) Electromagnetic interference shielding performance of polyurethane composites: A comparative study of GNs-IL/Fe 3 O 4 and MWCNTs-IL/Fe 3 O 4 hybrid fillers. Compos Part B Eng 164:467–475. https://doi.org/10.1016/j.compositesb.2019.01.062
19. Zhang N, Huang Y, Wang M (2018) 3D ferromagnetic graphene nanocomposites with ZnO nanorods and Fe3O4 nanoparticles co-decorated for efficient electromagnetic wave absorption. Compos Part B Eng 136:135–142. https://doi.org/10.1016/j.compositesb.2017.10.029
20. Issa B, Obaidat IM, Albiss BA, Haik Y (2013) Magnetic nanoparticles: Surface effects and properties related to biomedicine applications. Int J Mol Sci 14:21266–21305. https://doi.org/10.3390/ijms141121266
21. Bronnikov S, Kostromin S, Asandulesa M, et al (2020) Interfacial interactions and interfacial polarization in polyazomethine/MWCNTs nanocomposites. Compos Sci Technol 190:108049. https://doi.org/10.1016/j.compscitech.2020.108049
22. Gill N, Gupta V, Tomar M, et al (2020) Improved electromagnetic shielding behaviour of graphene encapsulated polypyrrole-graphene nanocomposite in X-band. Compos Sci Technol 192:108113. https://doi.org/10.1016/j.compscitech.2020.108113
23. Bouhfid R, Essabir H, El Kacem Qaiss A (2016) Graphene-Based Nanocomposites: Mechanical, Thermal, Electrical, and Rheological Properties. In: Rheology and Processing of Polymer Nanocomposites. wiley, pp 405–430
24. Essabir H, Raji M, Bouhfid R, Qaiss A el kacem (2019) Rheological Properties of Functionalized Graphene and Polymeric Matrices–Based Nanocomposites. In: Functionalized Graphene Nanocomposites and their Derivatives. Elsevier, pp 109–120
25. Raji M, Essabir H, Essassi EM, et al (2016) Morphological, Thermal, Mechanical, and Rheological Properties of High Density Polyethylene Reinforced With Illite Clay. Polym Polym Compos 16:101–113. https://doi.org/10.1002/pc
26. Essabir H, Hilali E, El Minor H, et al (2015) Mechanical and thermal properties of polymer composite based on natural fibers: Moroccan Luffa sponge/high density polyethylene. J Biobased Mater Bioenergy 9:. https://doi.org/10.1166/jbmb.2015.1524
27. Tiouitchi G, Raji M, Mounkachi O, et al (2019) Black phosphorus-based polyvinylidene fluoride nanocomposites: Synthesis, processing and characterization. Compos Part B Eng 175:107165. https://doi.org/10.1016/j.compositesb.2019.107165

28. Raji M, Essabir H, Bouhfid R, El Kacem Qaiss A (2017) Impact of chemical treatment and the manufacturing process on mechanical, thermal, and rheological properties of natural fibers-based composites. In: Handbook of Composites from Renewable Materials. wiley, Hoboken, NJ, USA, pp 225–252
29. ISO 527-1:2012. Plastics-determination of tensile properties -Part 1: General principles ISO 527-1:2012. Plastics-determination of tensile properties -Part 1: General principles
30. Kausar A (2018) A review of filled and pristine polycarbonate blends and their applications. J Plast Film Sheeting 34:60–97. https://doi.org/10.1177/8756087917691088
31. Qaiss AEK, Bouhfid R, Essabir H (2014) Natural fibers reinforced polymeric matrix: Thermal, mechanical and interfacial properties
32. Qaiss A, Bouhfid R, Essabir H (2015) Characterization and use of coir, almond, apricot, argan, shells, and wood as reinforcement in the polymeric matrix in order to valorize these products
33. Essabir H, El Mechtali FZ, Nekhlaoui S, et al (2020) Compatibilization of PA6/ABS blend by SEBS-g-MA: morphological, mechanical, thermal, and rheological properties. Int J Adv Manuf Technol 110:1095–1111. https://doi.org/10.1007/s00170-020-05888-5
34. Raji M, Essabir H, Rodrigue D, et al (2018) Influence of graphene oxide and graphene nanosheet on the properties of polyvinylidene fluoride nanocomposites. Polym Compos 39:2932–2941. https://doi.org/10.1002/pc.24292
35. Udoetok I a, Wilson LD, Headley J V (2016) Stabilization of Pickering Emulsions by Iron oxide Nano-particles. Adv Mater Sci 1:24–33. https://doi.org/10.15761/AMS.1000107
36. Greco A, Timo A, Maffezzoli A (2012) Development and characterization of amorphous thermoplastic matrix graphene nanocomposites. Materials (Basel) 5:1972–1985. https://doi.org/10.3390/ma5101972
37. Essabir H, Nekhlaoui S, Bensalah MO, et al (2017) Phosphogypsum Waste Used as Reinforcing Fillers in Polypropylene Based Composites: Structural, Mechanical and Thermal Properties. J Polym Environ 25:. https://doi.org/10.1007/s10924-016-0853-9
38. Essabir H, Bensalah MO, Bouhfid R, Qaiss A (2014) Fabrication and characterization of apricot shells particles reinforced high density polyethylene based bio-composites: Mechanical and thermal properties. J Biobased Mater Bioenergy 8:. https://doi.org/10.1166/jbmb.2014.1447
39. Mekhzoum MEM, Essabir H, Rodrigue D, et al (2016) Graphene/Montmorillonite Hybrid Nanocomposites Based on Polypropylene: Morphological, Mechanical, and Rheological Properties. Polym Compos 16:101–113. https://doi.org/10.1002/pc
40. Yusuf M, Kumar M, Khan MA, et al (2019) A review on exfoliation, characterization, environmental and energy applications of graphene and graphene-based composites. Adv. Colloid Interface Sci. 273:102036
41. Alam MF, Khan MS, Uddin I, et al (2020) Exfoliation synthesis of graphene and optimization with alkali halides salts. Surfaces and Interfaces 20:100548. https://doi.org/10.1016/j.surfin.2020.100548

42. Yin PT, Shah S, Chhowalla M, Lee KB (2015) Design, synthesis, and characterization of graphene-nanoparticle hybrid materials for bioapplications. Chem Rev 115:2483–2531. https://doi.org/10.1021/cr500537t
43. Nekhlaoui S, Abdelaoui H, Raji M, et al (2021) Assessment of thermo-mechanical, dye discoloration, and hygroscopic behavior of hybrid composites based on polypropylene/clay (illite)/TiO2. Int J Adv Manuf Technol. https://doi.org/10.1007/s00170-021-06765-5
44. Ma X, Tao H, Yang K, et al (2012) A functionalized graphene oxide-iron oxide nanocomposite for magnetically targeted drug delivery, photothermal therapy, and magnetic resonance imaging. Nano Res 5:199–212. https://doi.org/10.1007/s12274-012-0200-y
45. Bensalah H, Raji M, Abdellaoui H, et al (2021) Thermo-mechanical properties of low-cost “green” phenolic resin composites reinforced with surface modified coir fiber. Int J Adv Manuf Technol 1–14. https://doi.org/10.1007/s00170-020-06535-9
46. Laaziz SA, Raji M, Hilali E, et al (2017) Bio-composites based on polylactic acid and argan nut shell: Production and properties. Int J Biol Macromol 104:. https://doi.org/10.1016/j.ijbiomac.2017.05.184
47. Al-itry R, Lamnawar K, Maazouz A (2015) Biopolymer Blends Based on Poly (lactic acid): Shear and Elongation Rheology/Structure/Blowing Process Relationships. https://doi.org/10.3390/polym7050939
48. Bensalah H, Gueraoui K, Essabir H, et al (2017) Mechanical, thermal, and rheological properties of polypropylene hybrid composites based clay and graphite. J Compos Mater 51:3563–3576. https://doi.org/10.1177/0021998317690597
49. Galpaya D, Wang M, Liu M, et al (2012) Recent Advances in Fabrication and Characterization of Graphene-Polymer Nanocomposites
50. Li T, Meng Z, Keten S (2020) Interfacial mechanics and viscoelastic properties of patchy graphene oxide reinforced nanocomposites. Carbon N Y 158:303–313. https://doi.org/10.1016/j.carbon.2019.10.039
51. Essabir H, Rodrigue D, Bouhfid R, Qaiss A e. K (2016) Effect of nylon 6 (PA6) addition on the properties of glass fiber reinforced acrylonitrile-butadiene-styrene. Polym Compos. https://doi.org/10.1002/pc.23895
52. Boujmal R, Essabir H, Nekhlaoui S, et al (2014) Composite from polypropylene and henna fiber: Structural, mechanical and thermal properties. J Biobased Mater Bioenergy 8:. https://doi.org/10.1166/jbmb.2014.1420
53. Essabir H, Bensalah MO, Rodrigue D, et al (2016) Biocomposites based on Argan nut shell and a polymer matrix: Effect of filler content and coupling agent. Carbohydr Polym 143:70–83. https://doi.org/10.1016/j.carbpol.2016.02.002
54. Nekhlaoui S, Essabir H, Kunal D, et al (2014) Comparative Study for the Talc and Two Kinds of Moroccan Clay as Reinforcements in Polypropylene-SEBS-g-MA Matrix. Polym Compos 10:. https://doi.org/10.1002/pc

55. Kim H, Abdala A a., MacOsko CW (2010) Graphene/polymer nanocomposites. Macromolecules 43:6515–6530. https://doi.org/10.1021/ma100572e
56. Adrar S, Habi A, Ajji A, Grohens Y (2017) Applied Clay Science Combined e ff ect of epoxy functionalized graphene and organomontmorillonites on the morphology , rheological and thermal properties of poly (butylenes adipate- co -terephtalate) with or without a compatibilizer. Appl Clay Sci 146:306–315. https://doi.org/10.1016/j.clay.2017.06.009
57. Zeng S, Li X, Li M, et al (2019) Flexible PVDF/CNTs/Ni@CNTs composite films possessing excellent electromagnetic interference shielding and mechanical properties under heat treatment. Carbon N Y 155:34–43. https://doi.org/10.1016/j.carbon.2019.08.024
58. Yadav RS, Kuritka I, Vilcáková J, et al (2019) Polypropylene nanocomposite filled with spinel ferrite NiFe 2 O 4 nanoparticles and in-situ thermally-reduced graphene oxide for electromagnetic interference shielding application. Nanomaterials 9:. https://doi.org/10.3390/nano9040621
59. Georgakilas V, Tiwari JN, Kemp KC, et al (2016) Noncovalent Functionalization of Graphene and Graphene Oxide for Energy Materials , Biosensing , Catalytic , and Biomedical Applications. Chem Rev 116:5464–5519. https://doi.org/10.1021/acs.chemrev.5b00620
60. Erukhimovich I, de la Cruz MO (2004) Phase equilibria and charge fractionation in polydisperse polyelectrolyte solutions. 2097–2112. https://doi.org/10.1002/polb
61. Uchiyama, MK, Toma, SH, Rodrigues, SF, Shimada, AL, Loiola, RA, Cervantes Rodríguez, HJ, Oliveira, PV, Luz, M, Rabbani, SR, Toma, HE, Poliselli Farsky, SH, Araki K (2015) Ultrasmall cationic superparamagnetic iron oxide nanoparticles as nontoxic and efficient MRI contrast agent and magnetic-targeting tool. Uchiyama MK1, Toma SH1, Rodrigues SF2, Shimada AL2, Loiola RA2, Cervantes Rodríguez HJ3, Oliveira PV4, Luz MS4, Rabban. Int J Nanomedicine 10:4731–46. https://doi.org/10.2147/IJN.S83150 M4 - Citavi
62. Campos CH, Urbano BF, Rivas BL (2014) Synthesis and characterization of organic–inorganic hybrid composites from poly(acrylic acid)-[3-(trimethoxysilyl)propyl methacrylate]-Al2O3. Compos Part B Eng 57:1–7. https://doi.org/10.1016/j.compositesb.2013.09.031
63. Chen Y, Xianyu Y, Wu J, et al (2016) Click chemistry-mediated nanosensors for biochemical assays. Theranostics 6:969–985. https://doi.org/10.7150/thno.14856
64. Ridi F, Bonini M, Baglioni P (2014) Magneto-responsive nanocomposites: Preparation and integration of magnetic nanoparticles into films, capsules, and gels. Adv. Colloid Interface Sci. 207:3–13

Figures

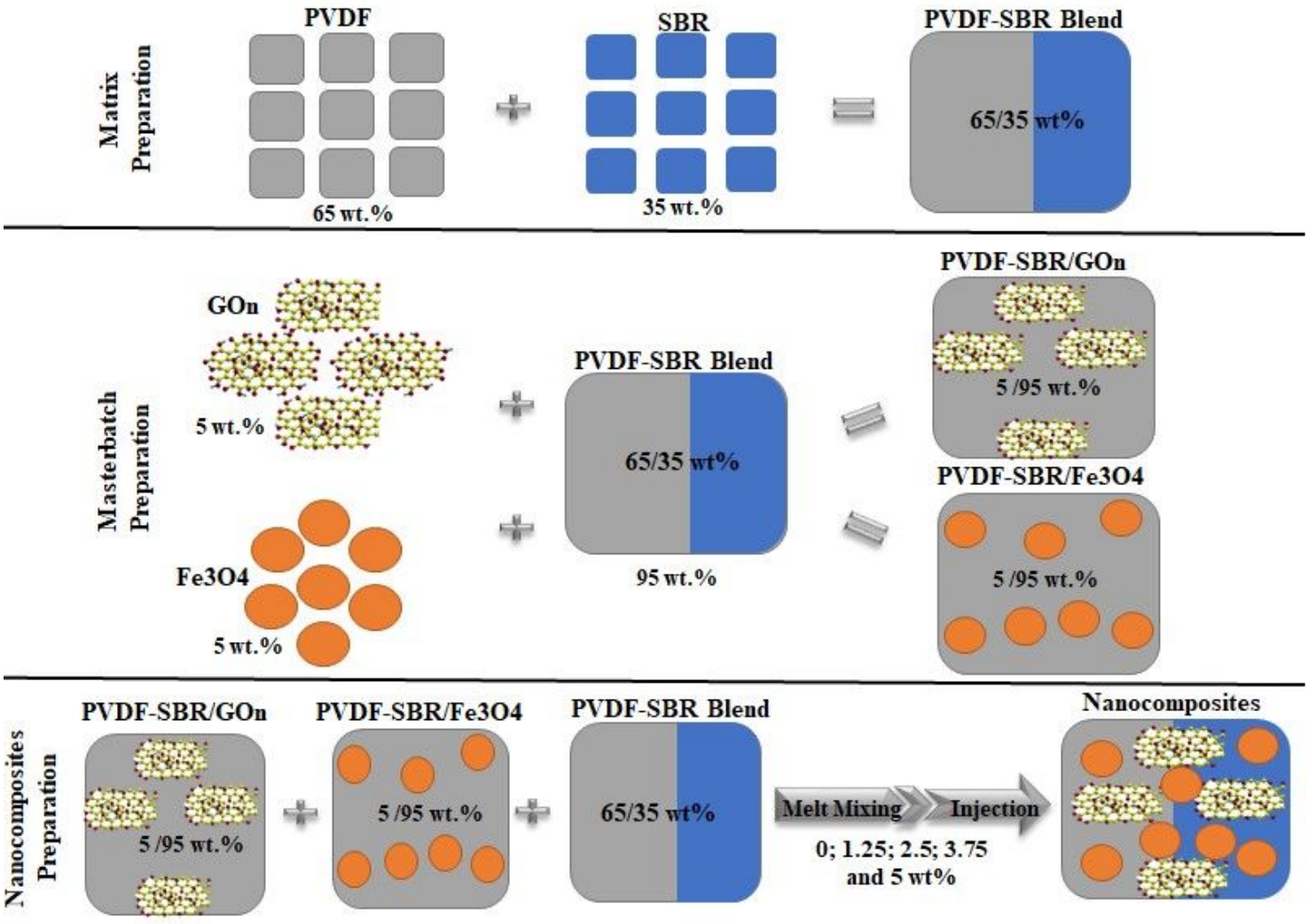

Figure 1

Schematic illustration of the preparation steps for the PVDF-SBR nanocomposites with iron oxide nanoparticles and graphene oxide nanosheets at different nanoparticles content.

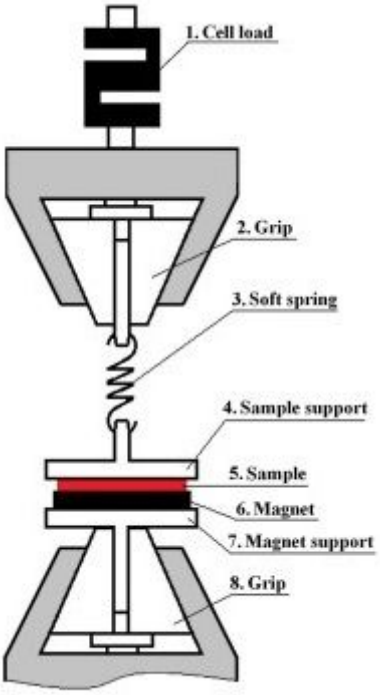

Figure 2

Schematic representation of the setup developed to characterize the magnetic strength of the nanocomposites [25].

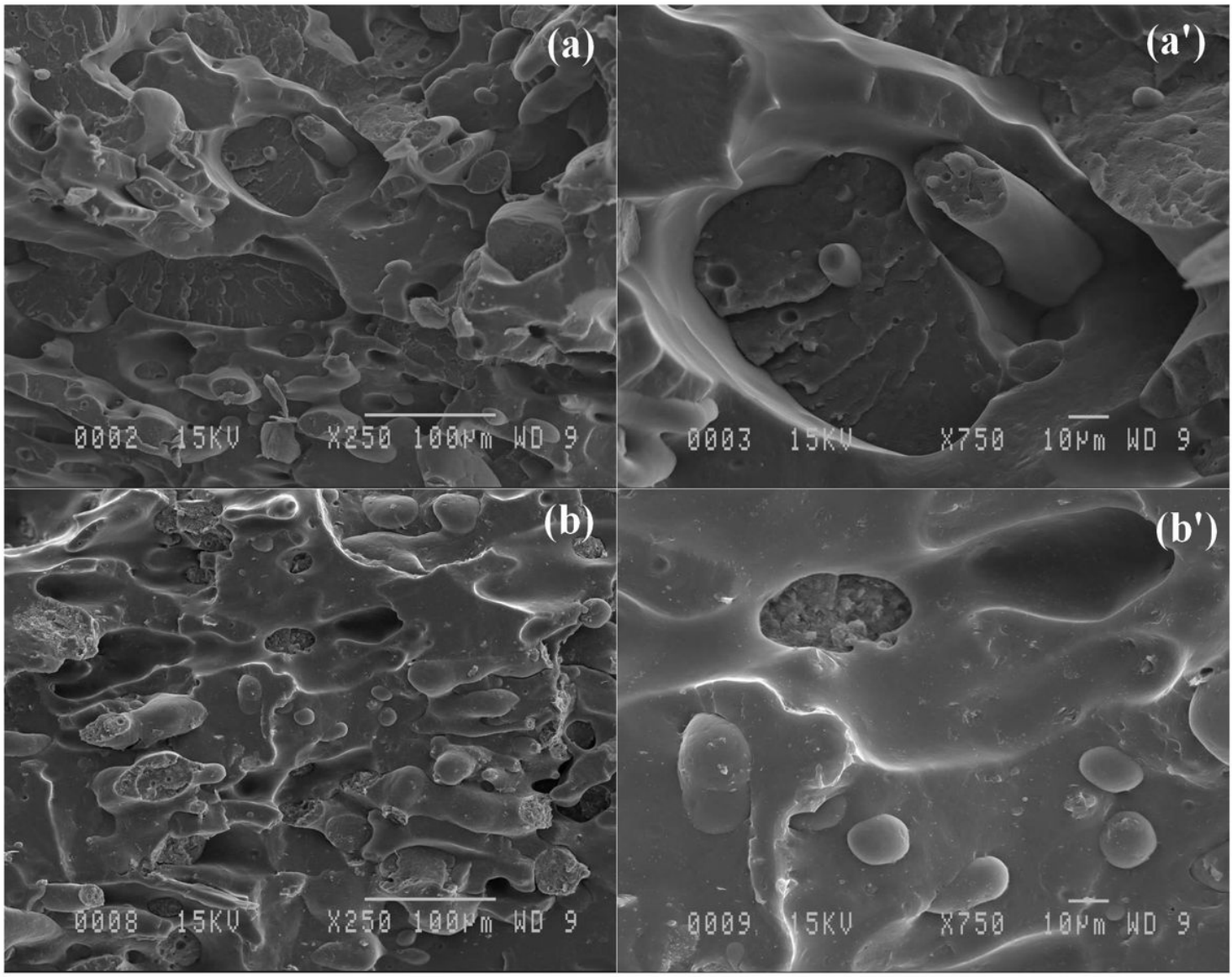

Figure 3

SEM images of : (a, a') the neat PVDF-SBR blend and (b, b') a typical nanocomposite (GOn-Fe3O4 at 2.5-2.5 wt.%).

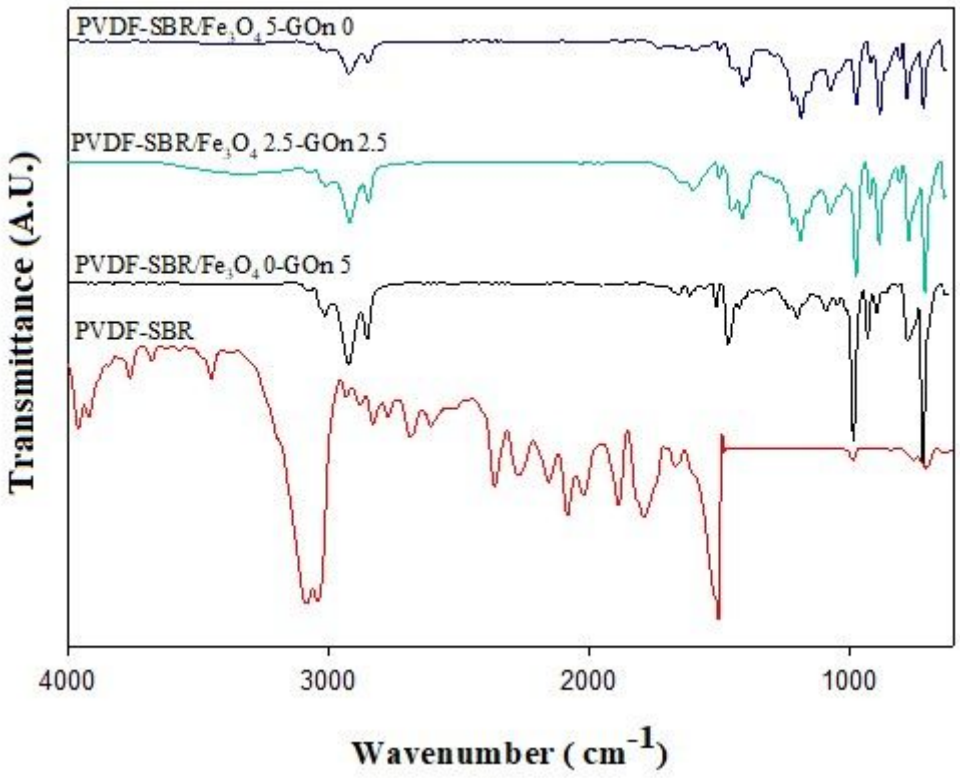

Figure 4

FTIR spectra of the neat PVDF-SBR blend and its nanocomposites.

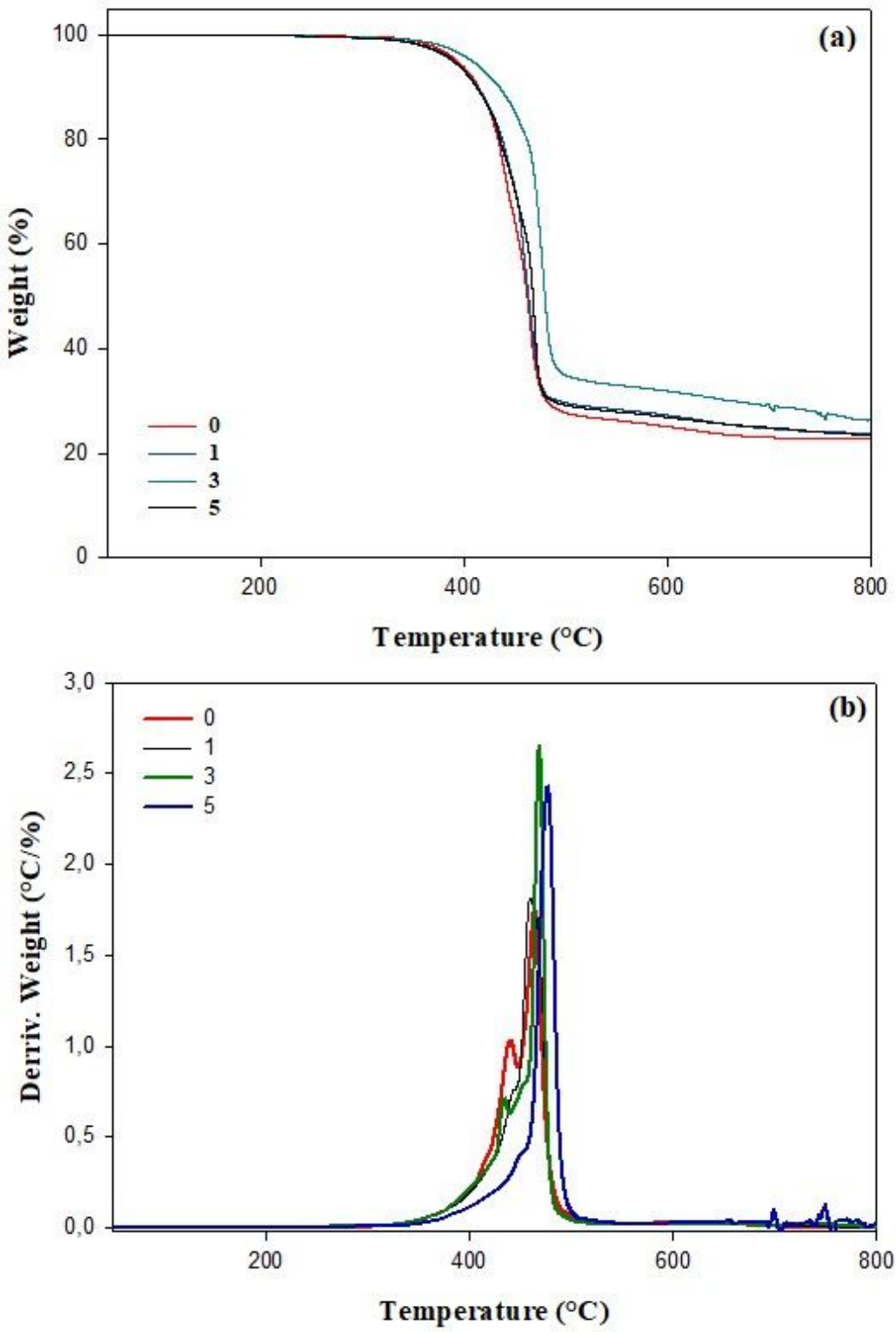

Figure 5

Thermogravemetric analysis of the neat PVDF-SBR blend and its nanocomposites : (a) TGA, and (b) DTG curves.

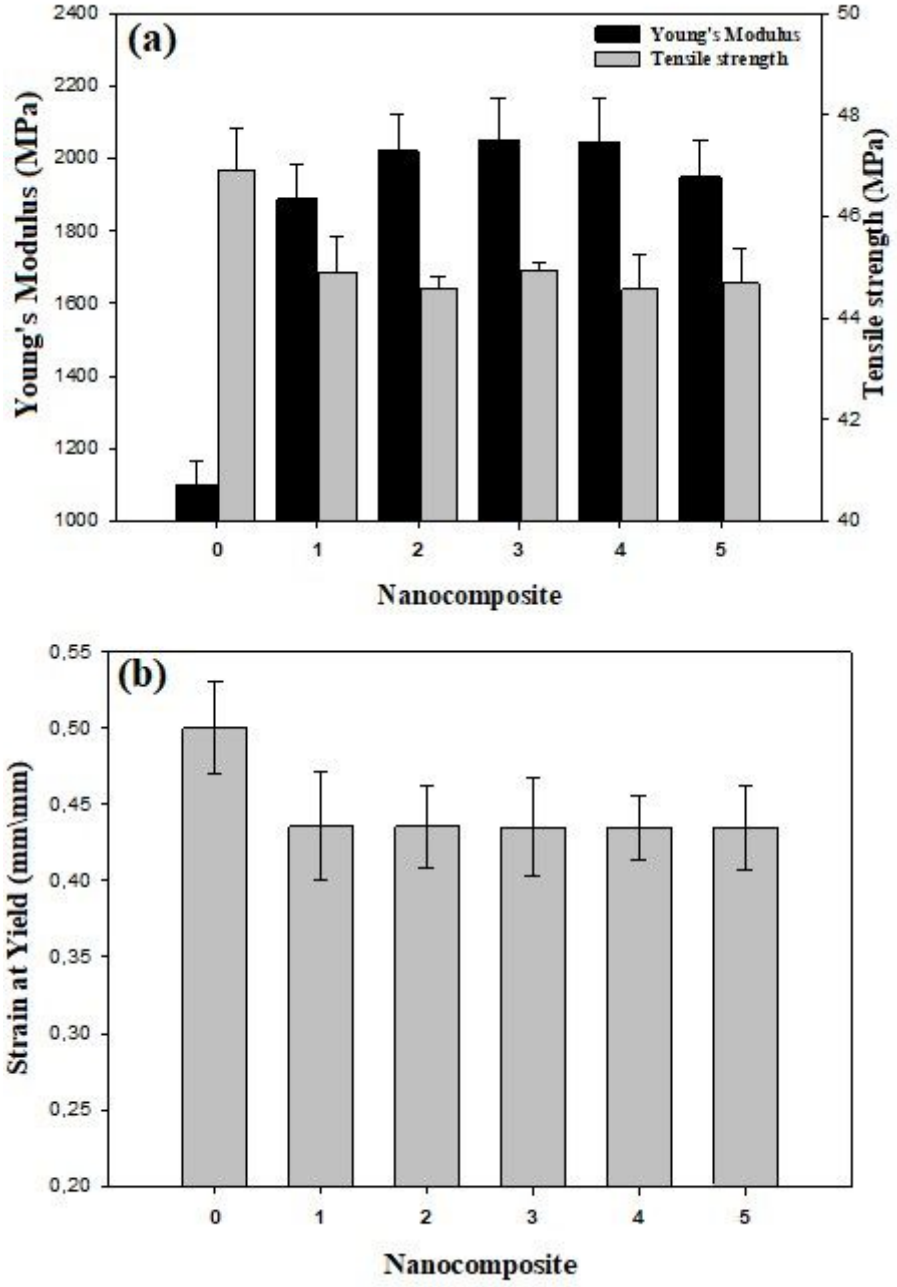

Figure 6

Tensile properties of the neat PVDF-SBR blend and its nanocomposites.

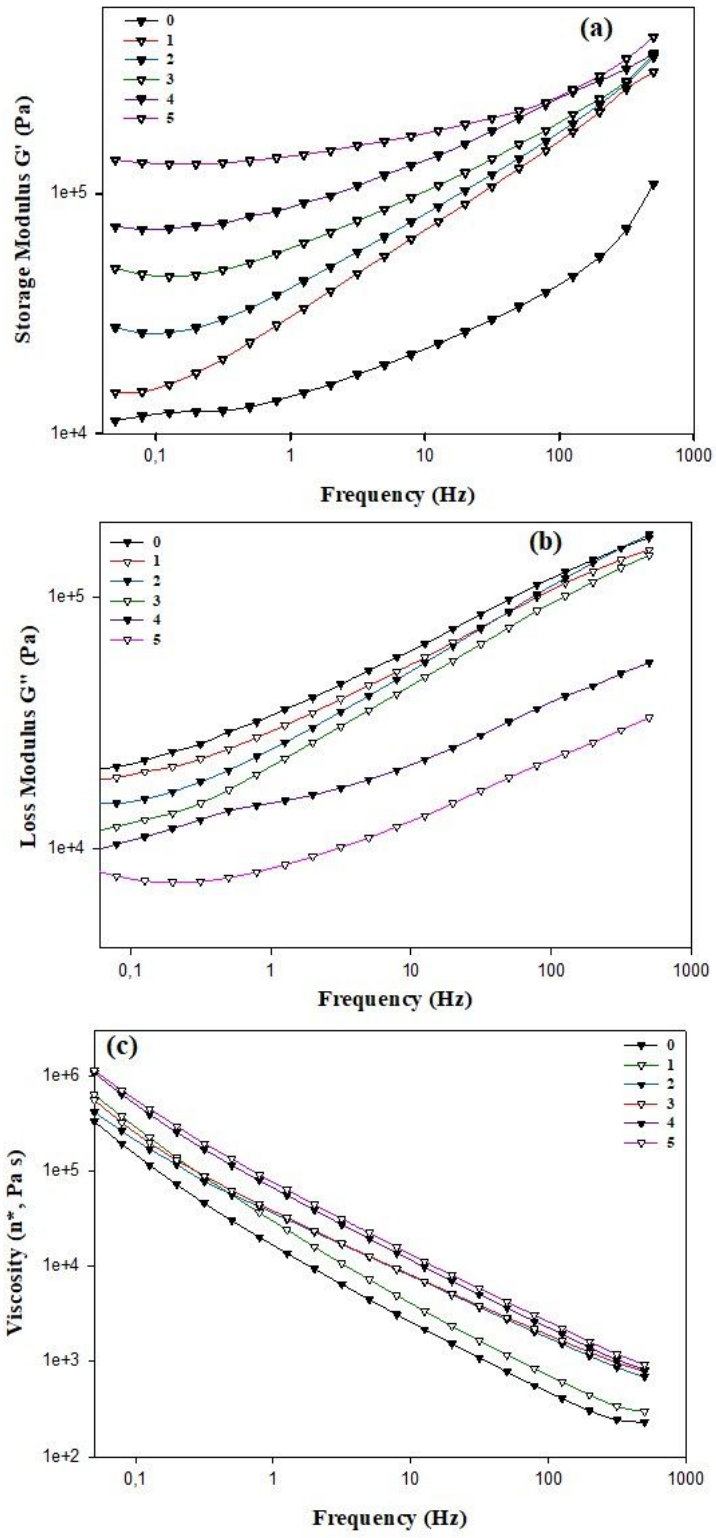

Figure 7

Rheological properties of the neat PVDF-SBR blend and its nanocomposites.

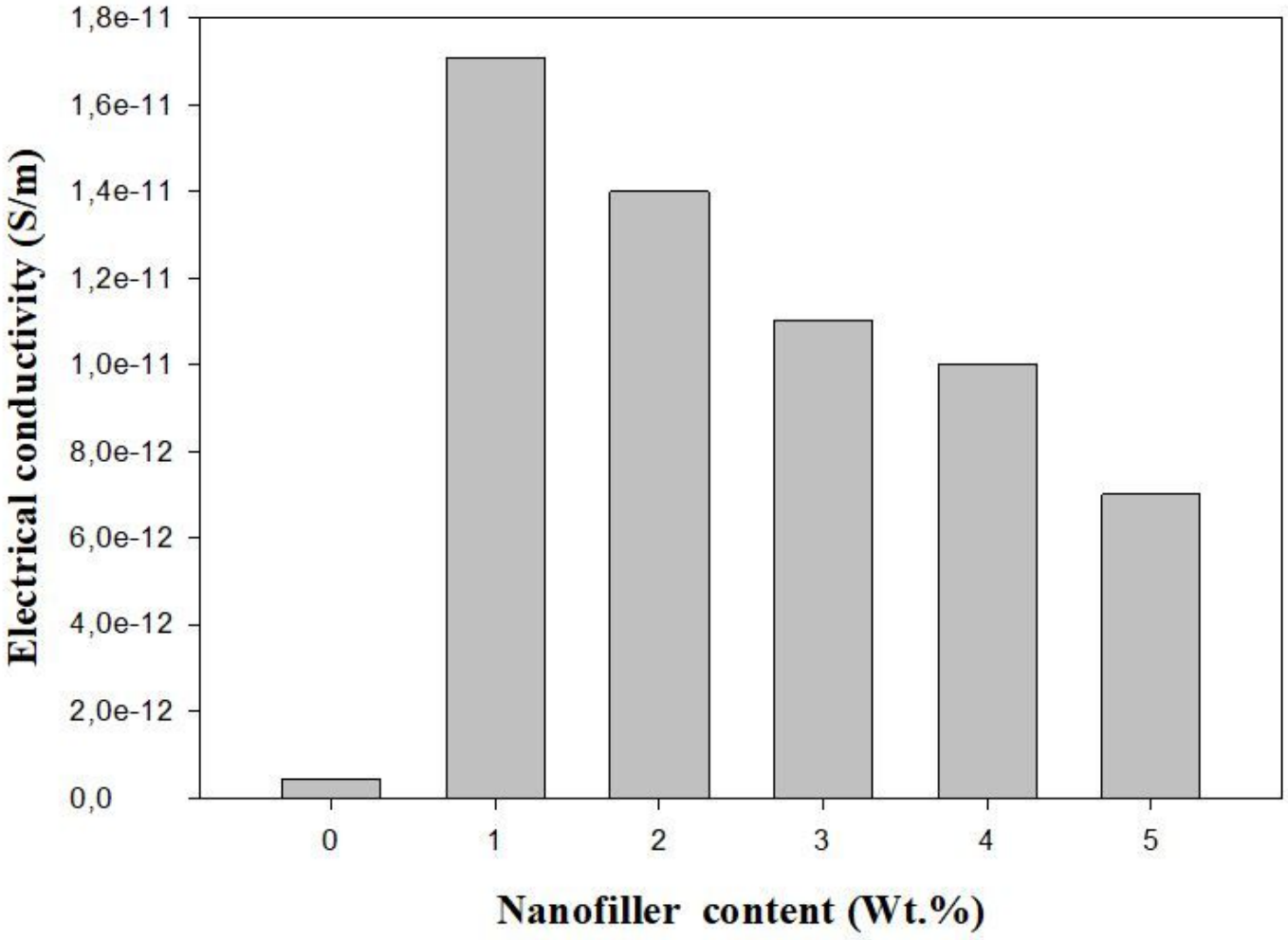

Figure 8

Electrical conductivity of the neat PVDF-SBR blend and its nanocomposites.

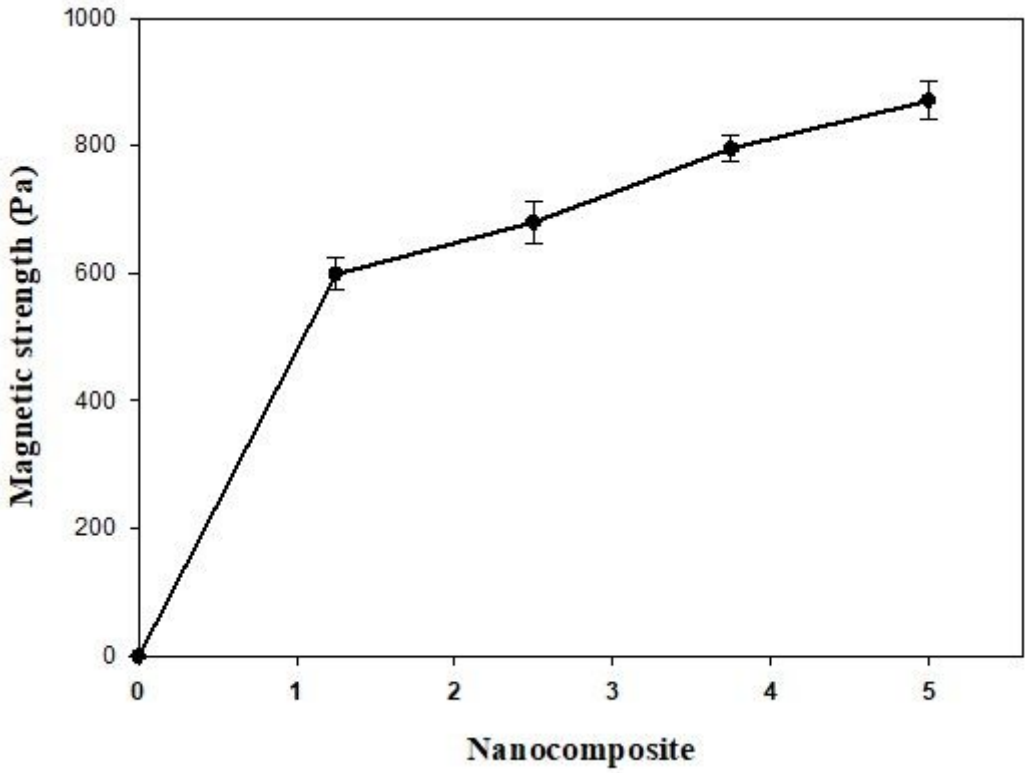

Figure 9

Magnetic properties of the neat PVDF-SBR blend and its nanocomposites.